The wave-induced drift of objects of finite size

Q. Xiao[1], R. Calvert[2,4], S.Q. Yan[3], T. Adcock[1], T.S. van den Bremer[1,4]
[1]Department of Engineering Science, University of Oxford, Oxford, UK
[2]School of Engineering, University of Edinburgh, Edinburgh, UK
[3]School of Mathematics, Computer Science and Engineering, City, University of London, UK
[4]Department of Civil Engineering and Geosciences, TU Delft, Delft, Netherlands
Presenting author, email: qian.xiao@eng.ox.ac.uk

1 INTRODUCTION

An understanding of wave-induced transport on the ocean surface is critical for the marine ecosystem health and ocean-related industries. Example applications are transport of plastic, oil patches and large ice floes. An unrestrained object floating in a field of surface gravity waves will normally experience a net drift in the direction of wave propagation in addition to the oscillatory motion associated with the waves. The net drift typically only becomes relevant over time scales much longer than the wave period due to the relatively small drift speeds. Unlike an idealized fluid parcel[1], an object of finite size may display non-Lagrangian drift behaviour[2]. This study examines the time-averaged transport of floating objects under the influence of regular waves in deep water. By using a hybrid numerical model that employs a fully nonlinear potential-flow model to capture the wave field and a Navier-Stokes (NS) model to calculate the detailed flow patterns near objects, our model encompasses both viscous effects and nonlinear wave-body interactions. A group of objects with different size, draft (submergence) and shape are investigated in the presence and absence of viscosity in the simulations. Their effects on drift and the mechanisms involved are explored.

2 NUMERICAL MODEL

The hybrid model QaleFOAM, employed in this study, is based on domain-decomposition method, which couples the QALE-FEM (Quasi Arbitrary Lagrangian-Eulerian Finite Element Method) model with the two-phase incompressible Navier-Stokes (NS) model InterDyMFOAM in OpenFOAM[3]. The domain is divided into two parts: the large outer domain is simulated by QALE-FEM to capture the waves, and a small inner domain, near the floating object, is solved by the NS model. In the NS model, both the air and water phases are assumed incompressible, and the VOF (volume of fluid) method is used to identify the phases and their interfaces. The coupling approach employed in this paper is a one-way coupling, which means that at the interfaces, the NS model only takes as input the solutions of QALE-FEM solver but does not feed its solutions back. For the 2D simulations performed in this paper, the front and back interfaces in the NS domain are empty, and a laminar viscosity model is used. The right interface of the NS domain is equipped with a passive wave absorber[3]. The left interface of the NS domain is coupled with the QALE-FEM, where the wave generated in the QALE-FEM domain using a flap wavemaker is transferred into the NS domain. A similar wave absorber is also equipped in the left interface to absorb the reflected/radiated waves from the objects. Note that although we do not deal with roll motions in this abstract, i.e. the results below are obtained with the approximation that the objects are not allowed to rotate, the effects of rotation on drifts will be reported on in the presentation and future publication.

3 NUMERICAL RESULTS

Drift of fluid parcels: We consider ideal fluid parcels, regarded as infinitely small objects, on regular waves in deep water with two different frequencies (low frequency ω=4.09 rad/s and high frequency ω=7.85 rad/s). For each frequency, a series of waves are simulated with different wave amplitudes, corresponding to different wave steepnesses ranging from 0.03 to 0.13, and the horizontal drift velocities of fluid particles are calculated to make comparison with the theoretical Stokes drift. First shown in [1], the horizontal component of Stokes drift velocity $\bar{u}_{sd}$ is given by

$$\bar{u}_{sd} = a^2 \omega k e^{2kz} = \varepsilon^2 \frac{\omega}{k} e^{2kz}, \tag{1}$$

where a denotes wave amplitude, ω is angular frequency, k is wave number and $\varepsilon=ka$ is the wave steepness. The mean drift velocities of fluid particles in quasi-steady state are obtained by applying the best linear fit to its horizontal trajectory and determining the slope of the linear fit line. A comparison between the numerical results and theoretical Stokes drift is given in Fig.1. The theoretical Stokes drift is obtained by Eq. 1, in

which z is equal to the vertical position of the tracked particles z_p. A non-dimensional velocity $\bar{u}_p / c$, where $c=\omega/k$ is the phase speed of the waves, is employed. Excellent agreement is achieved between the numerical results and the theoretical solution for cases of both higher and lower frequencies with various wave steepnesses validating our model and confirming its ability to predict the drift velocity of an infinitely small object. Convergence tests of three target quantities (surface elevation η, mean Eulerian velocity u_E and drift rates $\bar{u}_p$ of a fluid parcel) have been carried out for both grid mesh resolution as well as the length of the relaxation zone. In the interest of brevity, the results are not shown here.

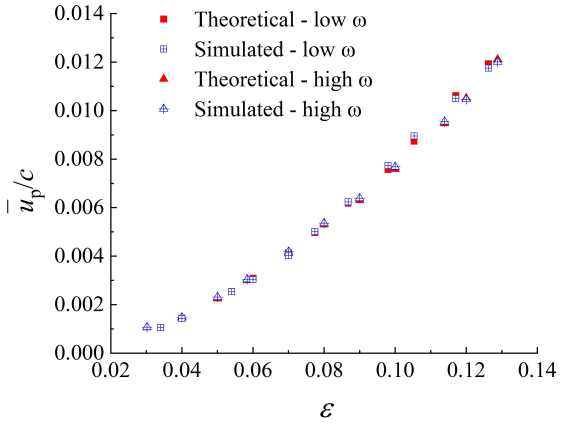

Figure 1 Horizontal drift velocities of fluid parcels.

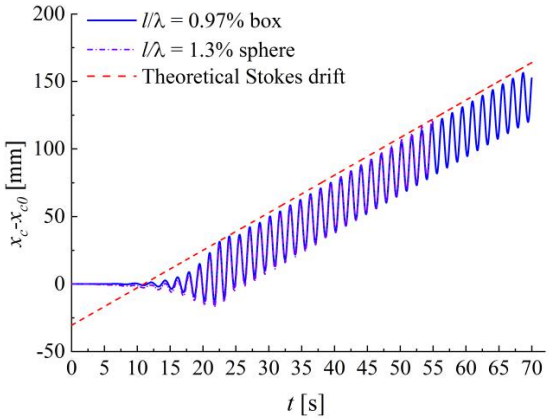

Figure 2 Example of horizontal trajectory of a small object.

Drift of very small objects: We next examine the drift of objects that are small relative to the wavelength but where there still is some wave/body interaction. Experiments support the intuition that when an object is small enough, its behaviour becomes purely Langrangian[4]. Two different object shapes are examined here: a rectangular box and a sphere. The wave condition is chosen from the above simulation as the case with ω=4.09 rad/s, ka=0.034. The size of the rectangular box is l=0.036 m (l/λ=1%), in which λ indicates the wavelength, l the length of the box in the direction of wave propagation. The diameter of the sphere is D =0.05 m (D/λ=1.3%). Both objects have the same density of ρ=500 kg/m^3. The height of the box and the radius of the sphere are chosen to make sure that the object will not be submerged by the waves.

The time history of the horizontal motion of the centre of mass x_c of both objects is given in Fig. 2 and compared with the theoretical Stokes drift. The initial position (t=0 s) of the centre of mass of the objects is given by x_{c0}. Satisfactory agreement is observed between the simulated results and the theoretical Stokes drift, validating the model and confirming that the drift of very small objects is equal to the Stokes drift.

Table 1 Scale parameters of the objects.

l/λ	1%	2%	3%	4%	5%	6%	7%	8%	9%	10%
D (m)	0.05	0.074	0.11	0.15	0.19	0.22	0.258	0.294	0.332	0.369
l (m)	0.036	0.074	0.11	0.15	0.19	0.22	0.258	0.294	0.332	0.369
h (m)	0.05	0.1	0.15	0.2	0.25	0.3	0.35	0.4	0.45	0.5

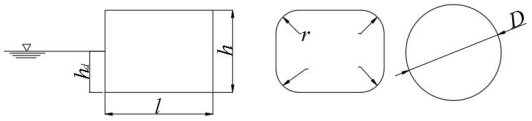

Sharp-cornered box Round-cornered box Sphere

Figure 3 Shapes of the objects.

Drift of objects of different sizes and shapes: Drift motions of objects of different sizes and shapes are examined here in the waves with low steepness. The shape of the objects along with the definitions of the scale parameters are given in Fig. 3. We define the following dimensionless parameters: relative object size is described by l/λ or D/λ; the radius of the corners of the round-cornered box is described by $r/(h/2)$, the density of all the objects ρ=500 kg/m^3. To investigate how size and shape of an object affect its transport and what role viscosity plays, we conduct a series of simulations with three object shapes and a range of sizes: a box with sharp corners, a box with round corners, and spheres. For the box with round corners, we set $r/(h/2)$=0.24. The relative size of objects, measured by wavelength, ranges from 1% up to 10% in 1%-point steps. The detailed scale parameters of the objects are given in Tab. 1. The difference between a sharp-

cornered box (SC) and round-cornered box (RC) is only the corner type, and the differences between a round-cornered box and a sphere (SP) with equivalent size are the submerged shape and submergence of the object. The simulations are performed with and without viscosity. Fig. 4 (a) provides the celerity-normalized drift velocity $\bar{u}_c / c$ as a function of relative object size. The vertical motion magnitudes Z_a are shown in Fig. 4 (b) as a function of relative object size, in which the magnitude is the time-averaged value after the quasi-steady state has been achieved.

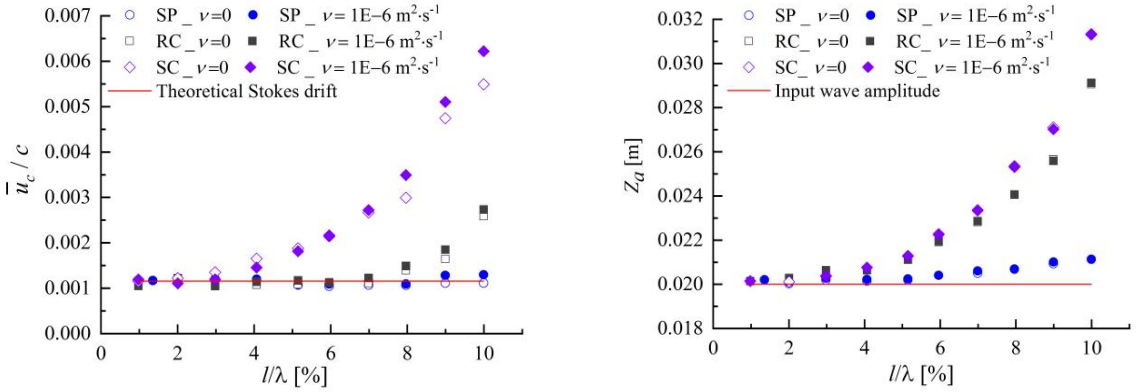

(a) Horizontal drift velocities of differently shaped objects (b) Vertical motion amplitude of differently shaped objects

Figure 4 Simulation results for different objects with viscosity (ν =10^{-6} m^2 · s^{-1}) and without viscosity (ν =0).

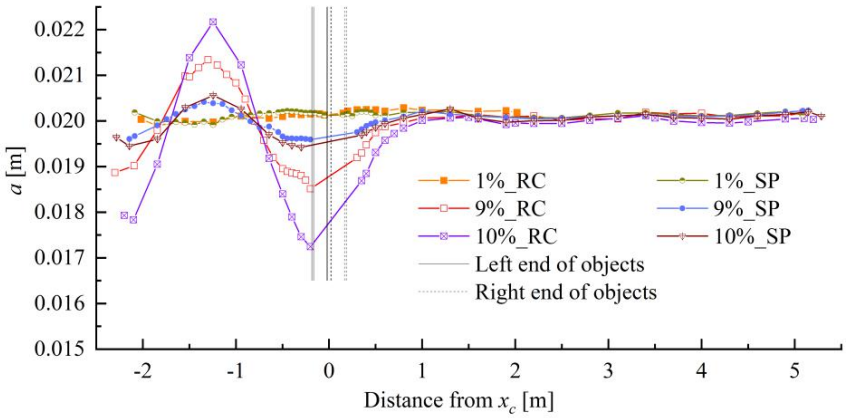

Figure 5 Distribution of amplitude of the surface elevation along horizontal direction

We start by examining the objects that experience the largest increases in drift, the group of sharp-cornered box (SC), as shown in Fig. 4 (a). We observe that when the box is very small, its drift rate is equal to the Stokes drift, while, as the box becomes larger, the drift speed is enhanced significantly along with an increase of the vertical motion magnitude. This phenomenon is clearly visible with and without viscosity. The enhanced drift is less observable for the cases of round-cornered box (RC) with relative size less than 7%, but becomes more discernible as size increases. The trends are similar whether or not viscosity is included. However, for spheres (SP), as depicted in the figure, no obvious enhancement of drift speed is found in the absence of viscosity even when the relative size is as large as 10%. In the presence of viscosity, small, enhanced drift is observed as the sphere becomes larger.

There is a large difference between the sharp-cornered boxes and the two other object types. Following scrutiny of the fluid fields during the simulations we found that, for sharp-cornered boxes, significant additional vorticity is generated around the sharp corners compared with the round-cornered boxes and the spheres, which manifest no obvious vorticity (no figures shown here for brevity). Although we do not explore the effect of vorticity in depth here, it is evident that the effects of flow separation, viscosity and vorticity are important factors in determining wave-induced drift. The discrepancy between the drift speeds of the round-cornered box and the sphere becomes large when the relative size of the object is larger than 7%. The increased drift is always accompanied by an increase of the amplitude of the vertical motion, as shown in the Fig. 4 (a) and (b). To further explain this phenomenon, we conduct an analysis of the wave field for round-cornered boxes and spheres. Fig. 5 depicts the wave amplitude as a function of the horizontal distance to the centre of mass of the objects for cases of 9% and 10% relative size for the round-cornered box (RC) and the sphere (SP). The results for 1% relative size are also given for comparison. A standing wave pattern

forms, and there are differences in the surface elevation amplitude on both sides of the objects; the differences are larger for larger boxes. This pattern is less clear for round-cornered boxes with a relative size smaller than 7% (not presented here for brevity) and for spheres, as seen in Fig. 5. This explains the previous observation that spheres in the absence of viscosity do not experience any observable increase in drift unlike the round-cornered boxes of equivalent size. The diffraction-based mechanism involved will be discussed further in the presentation and in future publications.

Here, we further examine the role played by viscosity. Compared with the result for spheres in the absence of viscosity (no significant drift increase for all sizes), enhanced drift becomes evident when the sphere is larger than 8% relative size and when viscosity is considered. For the round-cornered boxes, for which the standing wave pattern only comes into play for relatively large boxes, when this pattern is small, which is the case of objects smaller than 7% relative size, the presence of viscosity contributes to the drift increase in a way consistent with the spheres. As the round-cornered box becomes larger, the draft (submergence) of the box becomes larger, and the standing wave pattern becomes a dominant driver for drift increase. Viscosity works to promote the enhanced drift and yields a larger drift increase compared to the case without viscosity included.

For the sharp-cornered boxes, when the object has a relative size of 1%, viscosity has no influence on the drift, and drift is equal to the Stokes drift. For objects of relative size smaller than 5%, the presence of viscosity slightly reduces the drift enhancement, whereas for the cases of relative size larger than 6%, the drift velocity of the cases with viscosity included experience greater increase compared with their non-viscous counterparts. The influence of viscosity is a combination of its influence on vorticity and their effect on drift directly.

4 CONCLUSION

The effects that size, shape, and submergence impose on the mean drift motions of objects subjected to regular waves in deep water with low wave steepness are explored using a numerical model that both encompasses viscous effects and can model wave-body interaction. The results for fluid parcels and very small objects compare well with the theoretical Stokes drift. The simulations are carried out with and without viscosity for several different objects of different size, shape, and submergence. The dependence of mean drift rates on these factors is investigated. We identify two mechanisms that can explain increased drift, at a rate faster than the Stokes drift: viscosity and wave amplitude imbalance between the two sides of the object as part of a standing wave pattern resulting from diffraction by the object. Both these mechanisms come into play as the size of the object becomes larger. We note that our model is further validated by comparing the linear motion of the object and the surface elevation distribution with the results from a boundary element method. The results are consistent with the limited experimental evidence and analytical analysis[2,5-6]. Ongoing work concerning the effect of submerged shape and submergence on drift through diffraction will be reported on in the presentation.

Acknowledgement

This research work was supported by the China Scholarship Council-PAG Oxford Scholarship.

REFERENCES

[1] Stokes G G. 1880. *On the theory of oscillatory waves*. Transactions of the Cambridge philosophical society.

[2] Calvert, R., McAllister, M. L., Whittaker, C., Raby, A., Borthwick, A. G. L., & Van Den Bremer, T. S. 2021. *A mechanism for the increased wave-induced drift of floating marine litter*. Journal of Fluid Mechanics, 915.

[3] Yan, S., Wang, J., Wang, J., Ma, Q., & Xie, Z. 2020. *CCP-WSI blind test using qaleFOAM with an improved passive wave absorber*. International Journal of Offshore and Polar Engineering, 30(01), 43-52.

[4] Van Den Bremer, T. S., Whittaker, C., Calvert, R., Raby, A., & Taylor, P. H. 2019. *Experimental study of particle trajectories below deep-water surface gravity wave groups*. Journal of Fluid Mechanics, 879, 168-186.

[5] He, M., Ren, B., & Qiu, D. H. 2016. *Experimental study of nonlinear behaviors of a free-floating body in waves*. China Ocean Engineering, 30(3), 421-430.

[6] Huang, G., Law, A. W. K., & Huang, Z. 2011. *Wave-induced drift of small floating objects in regular waves*. Ocean Engineering, 38(4), 712-718.